Surface Structure of GaN(0001) in the Chemical Vapor Deposition Environment

A. Munkholm,[1] G. B. Stephenson,[2] J. A. Eastman,[2] C. Thompson,[2,3] P. Fini,[4] J. S. Speck,[4] O. Auciello,[2]
P. H. Fuoss,[5] and S. P. DenBaars[4]
[1]*Chemistry Division, Argonne National Laboratory, Argonne, Illinois 60439*
[2]*Materials Science Division, Argonne National Laboratory, Argonne, Illinois 60439*
[3]*Department of Physics, Northern Illinois University, DeKalb, Illinois 60115*
[4]*Materials Department, University of California, Santa Barbara, California 93106*
[5]*AT&T Laboratories—Research, Florham Park, New Jersey 07932*
(Received 22 December 1998)

We report the first observation of the atomic-scale structure of the GaN(0001) surface in the metal-organic chemical vapor deposition environment. Measurements were performed using *in situ* grazing-incidence x-ray scattering. We determined the surface equilibrium phase diagram as a function of temperature and ammonia partial pressure, which contains two phases with 1×1 and $(\sqrt{3} \times 2\sqrt{3})R30°$ symmetries. The $(\sqrt{3} \times 2\sqrt{3})R30°$ phase is found to have a novel "missing row" structure with 1/3 of the surface Ga atoms absent.

PACS numbers: 61.10.–i, 68.35.Bs, 81.15.Gh

Recent breakthroughs in the fabrication of devices such as blue light-emitting diodes [1], lasers [2], and high-power transistors [3] based on GaN and related nitrides have fueled an explosion of fundamental research on the synthesis, structure, and properties of these materials. Because knowledge of surface structure is critical to understanding thin film growth, the GaN surface

has recently been the focus of numerous experimental and theoretical studies [4–8]. The relatively large band gap, bond strength, ionicity, and atomic-size difference of GaN are expected to lead to surface reconstructions that differ from those encountered in "traditional" III-V semiconductors such as GaAs. In addition, the most common growth surface is the (0001) basal plane of wurtzite structure GaN, rather than the (001) cube face of zinc blende structure GaAs.

Although state-of-the-art GaN for optoelectronic devices is typically grown by metal-organic chemical vapor deposition (MOCVD), very little is known about the atomic-scale surface structure in the MOCVD environment. Current experimental understanding of GaN surface structure is based on studies in vacuum typical of the molecular-beam epitaxy (MBE) growth environment. Reconstructions of basal plane surfaces of wurtzite GaN in vacuum have recently been studied using scanning tunneling microscopy [4] and electron diffraction [4–6]. For GaN(0001) in vacuum, only 1×1, 2×2, and 5×5 reconstructions persist at typical growth temperatures. Structural models have been developed for the 1×1 and 2×2 reconstructions based on first-principles theory [4,7].

While these studies are directly applicable to MBE growth, there have been no previous measurements of GaN surface structure in the chemically complex MOCVD environment, where the growth chamber is at near-atmospheric pressure and the sample is surrounded by flows of precursors and carrier gasses, such as NH_3, trimethylgallium (TMG), N_2, and H_2. In this Letter we report the first observation of a GaN surface reconstruction in the MOCVD environment. The in-plane structure of the wurtzite GaN(0001) (Ga-face) surface was studied *in situ* by grazing-incidence x-ray scattering. We find that the surface structure at 200 Torr of NH_3, N_2, and H_2 differs from that in vacuum, having a reconstruction with a $(\sqrt{3} \times 2\sqrt{3})R30°$ symmetry which persists at temperatures up to at least 730 °C. We present the equilibrium surface phase diagram as a function of temperature and ammonia partial pressure $p(NH_3)$, and a solution of the structure of the $(\sqrt{3} \times 2\sqrt{3})R30°$ phase.

The samples consisted of 2-μm-thick GaN films grown on sapphire (0001) substrates using atmospheric-pressure MOCVD with a standard two-step process [9]. This growth process is known to produce a surface having the GaN(0001) polarity [10], which we confirmed using convergent-beam electron diffraction. X-ray scattering measurements were performed at the BESSRC undulator beam line 12-ID-D at the Advanced Photon Source, using a Si(111) monochromator set to 24 keV. The sample was mounted in a vertical-flow MOCVD chamber on a z-axis surface diffractometer designed for *in situ* x-ray scattering studies [11]. Incident and outgoing angles α and β were kept at the critical angle (0.12°). The in-plane mosaic width of the GaN films was 0.17°. After inserting a new sample, a 30-nm-thick homoepitaxial layer of GaN was grown *in situ* at 1000 °C using TMG and NH_3 as precursors. This step assures that the observed structure is intrinsic to the clean GaN(0001) surface, rather than due to air exposure of the initial sample. The temperature measurement was calibrated to an accuracy of ± 5 °C by monitoring the thermal expansion of a sapphire substrate via *in situ* optical interferometry.

We searched for surface reconstructions by performing in-plane radial scans along the $10\bar{1}0$ and $11\bar{2}0$ directions while the sample was held at temperatures up

to 1000 °C and $p(NH_3)$ between 2 and 140 Torr. The flow rate of the NH_3/carrier gas mixture directed at the sample was kept constant at 4.6 standard liters per minute with a total pressure of 200 Torr. Results presented here are from experiments using N_2 as the carrier gas; very similar results were obtained using H_2. At high temperatures, only the bulk peaks corresponding to a 1×1 structure were observed. At temperatures below 730 °C for $p(NH_3) = 140$ Torr [620 °C for $p(NH_3) = 2.2$ Torr] fractional-order diffraction peaks corresponding to a surface reconstruction appeared. After a few minutes, the widths of rocking curves through the reconstruction peaks indicated that the domain size had grown to 500 Å. Figures 1(a) and 1(b) show two typical in-plane scans in which 1/6-order peaks were observed. Reconstruction peaks were found at the positions shown in Fig. 1(c), which correspond to (and are here indexed according to) an apparent $(2\sqrt{3} \times 2\sqrt{3})R30°$ symmetry. However, this apparent symmetry would also be observed for a reconstruction with a $(\sqrt{3} \times 2\sqrt{3})R30°$ unit cell having multiple domains. The outlines of these unit cells along with the 1×1 unit cell are shown in Fig. 1(d). As discussed below, the best fit is in fact obtained for a $(\sqrt{3} \times 2\sqrt{3})R30°$ reconstruction.

We explored the reconstruction phase boundary by observing peak intensities while varying sample temperature and $p(NH_3)$. The result is shown in Fig. 2, where the shaded area corresponds to conditions under which the $(\sqrt{3} \times 2\sqrt{3})R30°$ phase is present. Unlike the surface phase diagram found for the vacuum environment [6] which shows multiple structures as a function of Ga coverage, we find only a single reconstruction over the entire range of $p(NH_3)$ typical of MOCVD. An increase in $p(NH_3)$ causes the transition between the $(\sqrt{3} \times 2\sqrt{3})R30°$ and 1×1 phases to shift to higher temperature. This transition was found to be reversible when changing either temperature or $p(NH_3)$. The fact that the transition was reproducible on all samples studied, which had surfaces grown under a variety of conditions, confirms that Fig. 2 represents the equilibrium phase diagram of a clean GaN surface. Equilibration times were rapid at high temperatures, but exceeded 10 min at temperatures below 600 °C. From the temperature dependence of $p(NH_3)$ at the transition, one can extract an apparent activation energy of 3.0 ± 0.2 eV. Assuming that the transition occurs at fixed nitrogen surface activity, and that N activity is determined by the ratio of

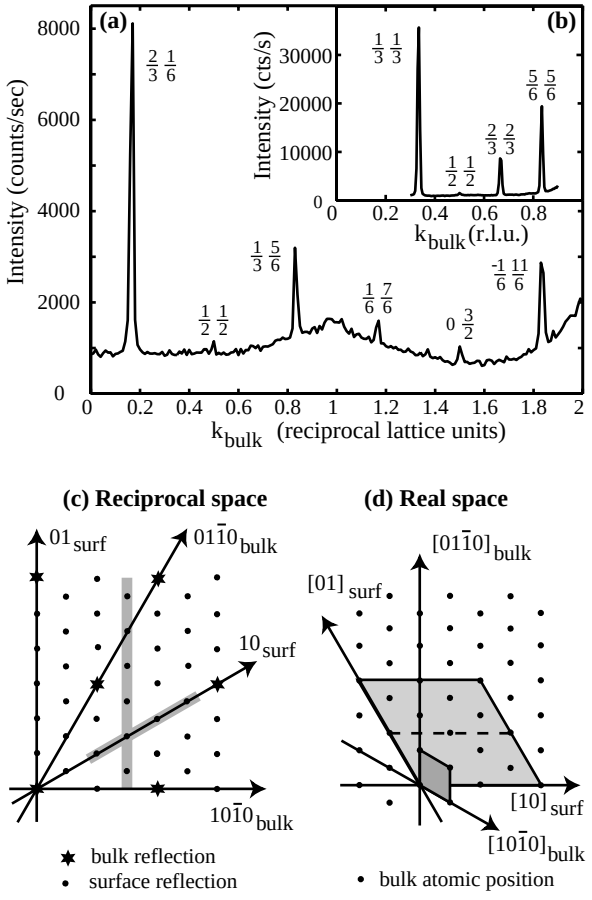

FIG. 1. (a) In-plane scan from $h_{bulk}, k_{bulk} = 0.75, 0$ to $-0.25, 2$ ($h_{bulk} = \frac{3}{4} - \frac{1}{2}k_{bulk}$). (b) In-plane radial scan from 0.3,0.3 to 0.9,0.9 ($h_{bulk} = k_{bulk}$). Sample is at 476 °C, $p(NH_3) = 140$ Torr. (c) Schematic of the observed symmetry of surface reconstruction peaks. Shaded lines correspond to scans shown in (a) and (b). (d) Schematic of unit cells for the GaN(0001) surface. The smaller diamond shows the 1×1 unit cell, and the larger diamond the $(\sqrt{3} \times 2\sqrt{3})R30°$ and $(2\sqrt{3} \times 2\sqrt{3})R30°$ unit cells.

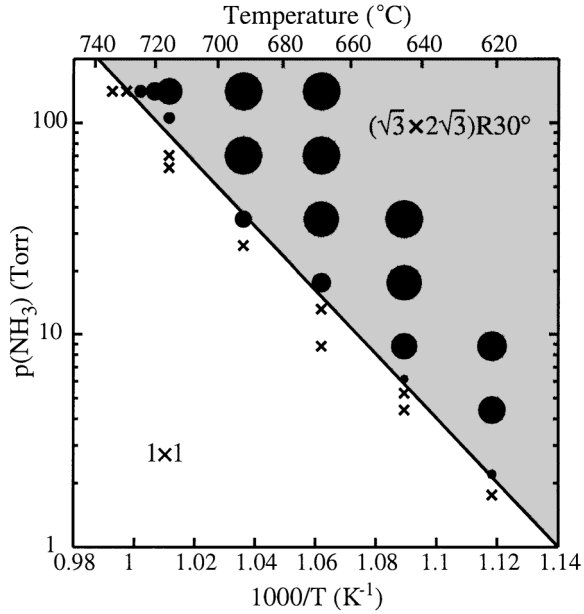

FIG. 2. Equilibrium phase diagram of the GaN(0001) surface under MOCVD conditions. Shaded area denotes conditions where the $(\sqrt{3} \times 2\sqrt{3})R30°$ reconstruction is observed. Solid circle areas are proportional to the intensity of the $\frac{1}{3}\frac{1}{3}_{bulk}(20_{surf})$ reflection measured under those conditions; crosses show conditions where this peak is not present.

impingement to desorption, one can interpret this value as the activation energy for desorption of the nitrogen species. In contrast, a study of the zinc blende GaN(001) surface in vacuum found an activation energy for N desorption of 6 eV [12].

Integrated intensities of ten or more reconstruction peaks were measured at 377, 476, and 715 °C. The intensity distribution remained nearly constant over this temperature range, indicating that there is little or no change in the atomic structure of the $(\sqrt{3} \times 2\sqrt{3})R30°$ phase. At 476 °C and $p(NH_3) = 140$ Torr we measured the integrated intensity of 25 symmetry-independent reconstruction peaks. We also measured several pairs of symmetry-related peaks and confirmed that the diffraction pattern exhibits reflection symmetry across the $(10)_{surf}$ and $(11)_{surf}$ directions in reciprocal space. The intensity distribution is shown in Fig. 3(a), where the filled half-circle areas are proportional to the measured intensities. The low-angle 10_{surf} peak was experimentally inaccessible because of background from the direct beam.

Several structural models having the appropriate symmetry were compared with the measured intensity distribution, including structures based on Si(111) $N \times N$ [13], GaAs(111) trimer [14], and "missing row" reconstructions. By far the best agreement was obtained for a novel missing row structure having a $(\sqrt{3} \times 2\sqrt{3})R30°$ unit cell where 1/3 of the top atomic layer is removed, so that four filled rows in the $[01]_{surf}$ direction are followed by two empty. Threefold rotation and reflection give six possible domain orientations. The diffraction pattern from this basis model has forbidden reflections at $h_{surf} - k_{surf} = 3n$. In the measured data, very weak reflections occur in this same pattern, indicating that the surface structure is closely related to this basis model. An inverse model, with two filled rows and four empty, gives the same diffraction pattern. However, fits allowing optimization of the atomic positions (as described below) found that the model with 2/3 of the atoms present is in significantly better agreement with the data. Other missing row models with, e.g., 5/6 or 1/2 occupancy do not produce the desired pattern of weak reflections.

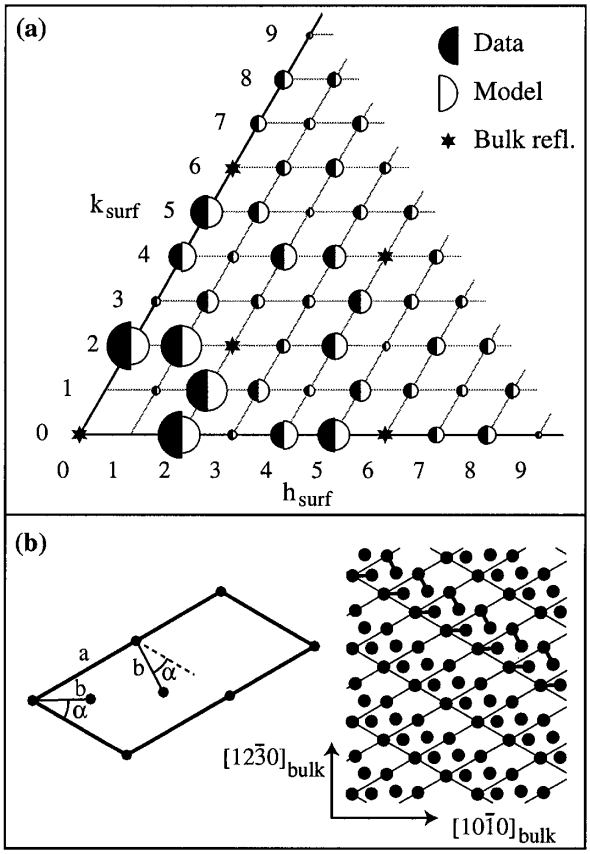

FIG. 3. (a) Filled and empty half circles show the measured intensities at 476 °C and the best fit calculated intensities, respectively, with areas proportional to the integrated intensity. (b) Schematic of the model parameters a, b, and α, and view of several unit cells drawn with the best-fit values.

Following standard procedures [15], refinement of the structural model was done by minimizing the residual $R_1 = \sum_{hk} w(\sqrt{I_{model}} - \sqrt{I_{meas}})^2 / \sum_{hk} w I_{meas}$, where w is the weight of each reflection. In calculating I_{model}, an isotropic Debye-Waller factor with mean-square atomic displacement u was used and an average was performed over the six domain orientations. Models with a partially filled layer of either Ga or N atoms were considered. First we allowed the positions of all four atoms in the unit cell to vary arbitrarily around the bulk lattice positions, as well as varying u and an overall scale factor. During this refinement, it became clear that the model converged towards a structure where symmetrical dimer rows are formed. Using a doubled $(2\sqrt{3} \times 2\sqrt{3})R30°$ unit cell with additional parameters did not significantly improve the fit. Thus, it was sufficient to use five fitting parameters: the dimer row separation a, the dimer bond length b, the angle α between the dimer and the row, the scale factor, and u. The best fit to the 476 °C data using Ga atoms was obtained for $a = 6.048$ Å, $b = 2.947$ Å, $\alpha = 31.7°$, and $u = 0.143$ Å, giving an R_1 value of 0.02. An equivalent fit was obtained using N atoms, with the same structural parameters except $u = 0.032$ Å. Figure 3(b) shows the "herringbone" pattern of dimers formed, and illustrates the three parameters a, b, and α. Compared with the corresponding values for atoms on the bulk lattice positions, the values found for these parameters vary only by factors of 1.096, 0.925, and 1.057, respectively. The formation of dimers and the slight expansion of the dimer row pair into the empty row appear to be physically quite reasonable. As shown in Fig. 3(a), we obtain overall good agreement between the best fit calculated from the model and the measured intensities, with only the low-index 20 reflection showing significant discrepancy. This discrepancy may be due to disorder which is not modeled well by the isotropic Debye-Waller factor, or to subsurface relaxation not included in the model.

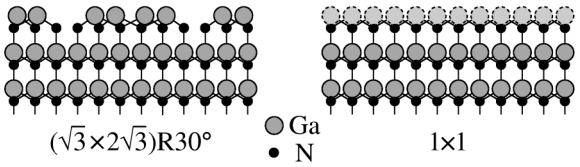

FIG. 4. Proposed cross sections of $(\sqrt{3} \times 2\sqrt{3})R30°$ and 1×1 structures, viewed along the $[01]_{\text{surf}}$ direction. Fractional occupancy of the 1×1 top Ga layer is indicated.

Because the variable scale and Debye-Waller factors could compensate for the difference in the atomic form factors, equally good fits could be obtained for models with a partially filled layer of either Ga or N. However, the value of the mean-square displacement u found for the Ga model (0.143 Å) is much more reasonable than that for the N model (0.032 Å), given a room-temperature value for the bulk crystal of 0.06 Å [16] and a typical surface-to-bulk ratio of about 3 [17]. Preliminary measurements of crystal truncation rod (CTR) scattering also support the Ga model. In particular, the integrated intensity of the strong 20 and 21 reconstruction peaks is approximately half that of the $11L$ CTR near $L = 1$ at high temperature in the 1×1 phase, which corresponds to the scattering from a single Ga-N bilayer. The ratio of these intensities should be about 0.4 for the Ga model, but only about 0.02 for the N model. Thus, we propose the out-of-plane structures shown in Fig. 4 for the $(\sqrt{3} \times 2\sqrt{3})R30°$ and 1×1 phases. The $(\sqrt{3} \times 2\sqrt{3})R30°$ structure consists of $1/3$ vacancies in the terminating Ga layer, ordered into rows. In the 1×1 phase, these vacancies are disordered. We also expect the fraction of Ga vacancies to decrease as temperature is increased at constant $p(NH_3)$ in the 1×1 phase, because N is more volatile than Ga [18].

Although *ab initio* calculations for the energies of various GaN(0001) surface structures performed to date have been based primarily on 1×1 and 2×2 symmetries in the vacuum environment, the proposed $(\sqrt{3} \times 2\sqrt{3})R30°$ structure is qualitatively consistent with present theory. Because of the high NH_3 partial pressure, the MOCVD environment corresponds to a very high N activity compared with typical vacuum environments. One of the most stable 2×2 reconstructions predicted for high N activities [4,7] is the Ga vacancy structure, in which the top Ga layer is $3/4$ occupied. This occupancy neutralizes the surface polarity without positional relaxation [19]. The $2/3$ occupancy of the proposed $(\sqrt{3} \times 2\sqrt{3})R30°$ structure is close to this condition. The remaining surface polarity could be accommodated by minor out-of-plane relaxation or by H adsorption. Since x-ray scattering measurements are insensitive to the presence of H, calculations could clarify its role in the $(\sqrt{3} \times 2\sqrt{3})R30°$ structure.

The $(\sqrt{3} \times 2\sqrt{3})R30°$ structure is directly relevant to understanding growth mechanisms of GaN at lower temperatures [20], such as those occurring during growth of barrier layers in $GaN/In_xGa_{1-x}N$ multi-quantum-well structures. More generally, this unique reconstruction provides the first example of the basal plane surface structure of a compound semiconductor in a reactive vapor-phase environment. The insight gained into the surface structures of GaN under a wide range of process conditions should provide a basis for further modeling of GaN surfaces and understanding of MOCVD growth mechanisms.

This work is supported by the National Science Foundation under Grant No. DMR-9704201, the State of Illinois under HECA, and the U.S. Department of Energy, BES-DMS under Contract No. W-31-109-ENG-38.

[1] S. Nakamura, T. Mukai, and M. Senoh, Appl. Phys. Lett. **64**, 1687 (1994).
[2] S. Nakamura *et al.*, Jpn. J. Appl. Phys. **35**, L74 (1996).
[3] U. K. Mishra *et al., Physics of Semiconductor Devices*, edited by V. Kumar and S. K. Agarwal (India Norosa, Delhi, 1998), Vol. II, p. 878.
[4] A. R. Smith *et al.*, Phys. Rev. Lett. **79**, 3934 (1997); A. R. Smith *et al.*, J. Vac. Sci. Technol. B **16**, 2242 (1998).
[5] P. Hacke *et al.*, Appl. Phys. Lett. **69**, 2507 (1996); X.-Q. Shen *et al.*, Jpn. J. Appl. Phys. **37**, L637 (1998).
[6] A. R. Smith *et al.*, Appl. Phys. Lett. **72**, 2114 (1998).
[7] J. E. Northrup, R. Di Felice, and J. Neugebauer, Phys. Rev. B **55**, 13 878 (1997); K. Rapcewicz, M. B. Nardelli, and J. Bernholc, Phys. Rev. B **56**, R12 725 (1997); J. Fritsch *et al.*, Phys. Rev. B **57**, 15 360 (1998).
[8] J. Neugebauer *et al.*, Phys. Rev. Lett. **80**, 3097 (1998); T. Zywietz, J. Neugebauer, and M. Scheffler, Appl. Phys. Lett. **73**, 487 (1998).
[9] X. H. Wu *et al.*, Jpn. J. Appl. Phys. **35**, L1648 (1996).
[10] J. L. Rouviere *et al.*, Appl. Phys. Lett. **73**, 668 (1998); E. S. Hellman, MRS Internet J. Nitride Semicond. Res. **3**, article 11 (1998).
[11] S. Brennan *et al.*, Nucl. Instrum. Methods Phys. Res., Sect. A **291**, 86 (1990); G. B. Stephenson *et al.*, MRS Bull. **24**(1), 21 (1999).
[12] O. Brandt, H. Yang, and K. H. Ploog, Phys. Rev. B **54**, 4432 (1996).
[13] R. J. Hamers, *Scanning Tunneling Microscropy I*, edited by H.-J. Güntherodt and R. Wiesendanger (Springer-Verlag, Berlin, 1992).
[14] E. Kaxiras *et al.*, Phys. Rev. Lett. **56**, 2819 (1986).
[15] *International Tables for X-ray Crystallography*, edited by J. S. Kaspar and K. Lonsdale (Kynoch, Birmingham, 1967), Vol. II, pp. 326–328.
[16] X. Xiong and S. C. Moss, J. Appl. Phys. **82**, 2308 (1997).
[17] F. J. Lamelas *et al.*, Phys. Rev. B **49**, 1957 (1994).
[18] D. D. Koleske *et al.*, J. Appl. Phys. **84**, 1998 (1998).
[19] A. Zangwill, *Physics at Surfaces* (Cambridge University, Cambridge, England, 1988), p. 105.
[20] G. B. Stephenson *et al.*, Appl. Phys. Lett. **74**, 3326 (1999).